Accepted Manuscript

Innovative ablative fire resistant composites based on phenolic resins modified with mesoporous silica particles

L. Asaro, L.B. Manfredi, S. Pellice, R. Procaccini, E.S. Rodriguez

PII: S0141-3910(17)30213-6

DOI: 10.1016/j.polymdegradstab.2017.07.023

Reference: PDST 8302

To appear in: *Polymer Degradation and Stability*

Received Date: 13 March 2017

Revised Date: 11 July 2017

Accepted Date: 19 July 2017

Please cite this article as: Asaro L, Manfredi LB, Pellice S, Procaccini R, Rodriguez ES, Innovative ablative fire resistant composites based on phenolic resins modified with mesoporous silica particles, *Polymer Degradation and Stability* (2017), doi: 10.1016/j.polymdegradstab.2017.07.023.

Innovative ablative fire resistant composites based on phenolic resins modified with mesoporous silica particles

L. Asaro[1], L. B. Manfredi[2], S. Pellice[3], R. Procaccini[4] and E. S. Rodriguez[1*]

[1] *Área de Materiales Compuestos, Instituto de Investigaciones en Ciencia y Tecnología de Materiales (INTEMA),UNMdP, CONICET, Facultad de Ingeniería, Av. Juan B Justo 4302, B7608FDQ, Mar del Plata, Argentina.*

[2] *Área de Ecomateriales, Instituto de Investigaciones en Ciencia y Tecnología de Materiales (INTEMA),UNMdP, CONICET, Facultad de Ingeniería, Av. Juan B Justo 4302, B7608FDQ, Mar del Plata, Argentina.*

[3] *Área de Cerámicos, Instituto de Investigaciones en Ciencia y Tecnología de Materiales (INTEMA),UNMdP, CONICET, Facultad de Ingeniería, Av. Juan B Justo 4302, B7608FDQ, Mar del Plata, Argentina.*

[4] *Área de Electroquímica Aplicada, Instituto de Investigaciones en Ciencia y Tecnología de Materiales (INTEMA),UNMdP, CONICET, Facultad de Ingeniería, Av. Juan B Justo 4302, B7608FDQ, Mar del Plata, Argentina.*

ABSTRACT

Mesoporous silica particles were used as reinforcement of a phenolic resin to develop new ablative materials. A resol type phenolic resin was filled with mesoporous silica particles synthesized from tetraethyl orthosilicate (TEOS). Samples of neat phenolic resin, phenolic resin reinforced with carbon black and with mesoporous silica particles (5 and 20 wt. %), were obtained. The ablative properties of the materials were studied by the oxyacetylene torch test and the ablated samples were observed by scanning electron microscopy (SEM). The composites were also characterized by dynamic mechanical analysis and transmission electron microscopy (TEM). Results showed a stronger chemical interaction between silica particles and the phenolic resin, than carbon black, thus increasing the glass transition temperature and mechanical properties of the silica/resin composites. In addition, the samples with mesoporous silica particles achieved lower erosion rates and back-face temperatures than the others, becoming promising thermal protection materials for the aerospace industry.

Keywords: Silica particles, Phenolic resin, Composite materials, Ablative materials, Thermal protection system.

*Corresponding author. To whom all correspondence should be addressed:
erodriguez@fi.mdp.edu.ar

1. INTRODUCTION

Thermal Protection System (TPS) materials are useful to assure the safe re-entry through the earth's atmosphere of space vehicle and missiles. Polymeric Ablative Materials (PAMs), generally based on high char retention resins such as phenolics, are the most versatile type of TPS materials [1]. However, char can be mechanically removed by friction action of atmospheric gases or to the rocket combustion products in such extremely conditions. So, a wide range of fibrous reinforcements is introduced in the polymeric binder to produce a Fiber Reinforced Polymeric Ablator (FRPA) [2]. Since the 1970s, the standard material used for thermal protection in the aerospace industry has been MX-4926, a rayon-based weave carbon fabric developed by NASA and produced by Cytec which is impregnated with phenolic resin and contains carbon black (50 wt. % carbon fibers, 35 wt. % phenolic resin, and 15 wt. % carbon black) [3]. However, current technologies of thermal protection systems have shown a threshold in their protection capacity that cannot be surpassed unless new materials are developed. Thus, novel ablative materials based on new matrices and new reinforcements have been studied in last years [4-9].

The use of new nano- and micron-sized reinforcements to reduce the erosion rate of the carbonaceous layer is one of the most common approaches [6, 10]. Wang et al. [8] studied the effect of carbon nanotubes in the ablative and mechanical properties of phenolic resin. They found that even low concentrations of carbon nanotubes with a good distribution in the matrix could make the materials more resistant to high temperature ablation. Natali et al. [2] investigated the ablative properties of multi-walled carbon nanotubes and carbon black-modified phenolic composites and found that both composites had better thermal stability than the neat resin and that the ablative response of the carbon black composite generated greater protection of the virgin

material. Pulci et al. [12] developed graphitic felt and graphitic foam phenolic composites and studied their thermal resistance. They found that optimization of the processing and curing is fundamental to achieve optimum materials; in the ablation test, both materials showed similar response but the felt composite passed undamaged during longer times, resulting in a better performance. Joseph H. Koo et al. [13] studied composites based on phenolic resin and nanoclay Cloisite 30B, carbon nanofibers and polyhedral oligomeric silsesquioxane to be used as ablative materials for solid rockets. The results showed that the carbon nanofiber composites allowed reaching the lowest erosion rate and the lowest back side temperature. Another approach that can be found in the literature is the use of silica particles to increase ablation resistance, based on their high thermal resistance. Aidin Mirzapour et. al. [14] studied the thermal stability and ablation properties of nanosilica (SiO_2) modified carbon fiber/phenolic composites. They found a reduction in the linear and mass erosion rate because of the silica. The microstructure investigation shows that nanoSiO_2 reacts with char at high-temperature, forming ablation resistant silicon carbide. R. Balaji et. al. [15] studied the thermal, thermo oxidation and ablative behavior of cenosphere filled ceramic/phenolic composites. The result shows that the thermal stability of the filled composites seems to be improved and reduction of mass loss was achieved with addition of cenosphere. Also the ablation results showed that the addition of cenosphere content exhibits the favorable ablation resistance of the composites. M. Natali et. al. [16] studied the ablative properties of nanosilica-based nanocomposites. They found that the silica nanoparticles melted when the temperature exceeded the filler melting point, thereby producing a viscous layer which acted as a high temperature binder that held the charred residue, which improves the effectiveness of the ablator.

However, despite the numerous researches conducted in the subject, there have not been significant advantages over the standard material.

In this work, we propose a new formulation based on phenolic resin modified with a different type of silica particles: mesoporous nanoparticles obtained by the sol-gel method [17] using tetraethyl orthosilicate as silica source. We expected that due to their high thermal resistance (characteristic of high purity silica) and the high internal porosity that reduces thermal conductivity, the ablation resistance of phenolic resin composites would be improved. Mesoporous silica particles have been used for drug delivery systems or for water treatment, but, to our knowledge, there are no studies where mesoporous silica particles are used to modify the thermal behavior of thermosetting resins [17-19].

The materials obtained in this work were studied in terms of ablation resistance, by means of the oxyacetylene torch test. Other properties such as glass transition temperature and modulus were measured by dynamic mechanical analysis (DMA) and the thermal degradation was studied by thermogravimetric analysis (TGA).

2. EXPERIMENTAL

2.1 Materials

2.1.1 Phenolic resin (Ph resin)

Resol-type phenolic resin was prepared using a formaldehyde-to-phenol molar ratio of 1.3 under basic conditions in a stainless steel reactor. After the synthesis the obtained resol was dehydrated in a rotary evaporator by vacuum at 70 ˚C. The synthesis procedure is explained in detail in a previous work [20]. Some characteristics of the resin are presented in **Table 1**.

2.1.2 Mesoporous silica particles

Ordered mesoporous silica nanoparticles were synthesized by the sol-gel method adapted from the procedure described by Bippus et al. [17]. In our case, 4.8 g of cetyltrimethylammonium bromide (CTAB, 99% from Aldrich) was dissolved in 192 ml of distilled water and heated at 30 ˚C with continuous stirring. Then, 102 ml of ethanol and 19.2 ml of ammonia (Cicarelli, 37%) were added to the mixture and kept under agitation for 10 min. After that, 7.65 ml of tetraethyl orthosilicate (98% from Aldrich) was added to the previous solution, and 35 s after the addition of tetraethyl orthosilicate, the reaction mixture was poured into 300 ml of distilled water and magnetic stirring was maintained. The solution (pH = 11) was neutralized for 180 s after dilution by adding a solution of 2 M HCl to reach a pH = 9.5, and then the stirring was stopped. At the end of the synthesis, a stable colloidal solution was obtained. The particles were washed with distilled water several times and then placed in a furnace for 24 h at 70 °C to attain the complete removal of the solvent, and the final heat treatment was performed in a muffle furnace with a heating rate of 5 °C/min, from room temperature to 600 °C and the maximum temperature was maintained during 4 hours. Finally, the particles were milled in a mortar to remove large agglomerates, to obtain a fine powder that was stored at room temperature until use.

2.1.3 Composites

Phenolic resin was synthesized with a formaldehyde-to-phenol molar ratio of 1.3, which is the ratio that allows obtaining the highest crosslinking density, and was selected in a previous work [21].

Composites were processed by compression molding.

Cured plates of phenolic resin, phenolic resin with mesoporous silica particles (5 wt. % and 20 wt. %), and phenolic resin with carbon black (Cabot Argentina SAIC) (5 wt. % and 20 wt. %) were obtained. First, the exact amounts of resin and reinforcements were weighed and mixed mechanically. The addition of a solvent (acetone) was necessary due to the large increase in resin viscosity associated with the addition of solid particles. Then, the blend was placed in an ultrasonic bath for 30 min at 60 °C and finally poured in a steel mold. The curing was done in two stages, the first part in an oven with the mold open (no pressure, 16 h at 80 °C), and the second part with the mold closed in a hydraulic press with 20 Bar and the following thermal cycle: 3 h at 100 ˚C, 3 h at 120 ˚C, 3 h at 150 ˚C and 4 h at 190 ˚C [20].

2.2. Methods

2.2.1 Characterization of the mesoporous particles and the composites.

Thermogravimetric tests were conducted in a Q500 TA Instruments equipment, from room temperature to 900 °C at a heating rate of 10 °C/min under a nitrogen and air atmosphere. Samples were about 10 mg.

X-ray diffraction (XRD) spectra were obtained in a PANalytical X´PERT PRO spectrometer, with CuK_α (λ=1.5406 Å) radiation at room temperature. The generator voltage was 40 kV and the current was 40 mA. Samples were tested at 10 °/min between 2 and 10 °.

Scanning electron microscopy (SEM) images were obtained in a JEOL JSM-6460LV microscope. The voltage used in the microscope was 15 kV, and magnification was 20X, 100X and 1000X. For this, the particles were dried and coated with a thin layer of gold (300 Å).

Transmission electron microscopy (TEM) images of the silica particles were obtained in a FE-TEM JEM-2100F, JEOL. And **TEM** images of the composites were obtained in a TEM JEOL 100 CX-II. Samples were ultramicrotomed at room temperature to give sections with a nominal thickness of 100 nm.

Fourier transform infrared (FTIR) spectra were obtained in a Nicolet 6700 spectrometer, in the Attenuated Total Reflectance mode. Tests were done at room temperature with 32 scans and 4 cm^{-1} of resolution.

Dynamic mechanical tests (DMA) were carried out in a Q800 TA Instruments equipment, in three-point bending mode. The frequency was set at 1 Hz, and the temperature ramp was from 30 to 350 °C at a heating rate of 5 °C/min.

Ablation testing. The ablation properties of the materials were measured by the oxyacetylene torch test (ASTM E285). The samples of 10x10x0.4 cm were placed at 1.9 cm of the torch and the back-face temperature of the samples was measured with a *K*-type thermocouple. The heat flow was obtained calibrating the torch with the procedure established in the ASTM E457 standard (Standard Test method for measuring heat-transfer rate using a thermal capacitance (slug) calorimeter).Copper was used as slug material and the temperature vs. time curve was measured (**Figure 1**).

The volumetric flow rate ratio oxygen/acetylene used was 1/2.4. Using the heat conduction equation proposed in the ASTM standard, a heat flux was 550 W/cm^2 was obtained.

3. RESULTS AND DISCUSSION

3.1 Mesoporous silica particles

TGA was conducted to choose the adequate thermal treatment for the mesoporous particles, and to find the temperature that ensures the total elimination of the surfactant (CTAB) remaining inside the pores. **Figure 1** shows the mass loss and its derivative versus temperature. Between 30 °C and 150 °C, there was a slight weight loss, attributed to free water removal; between 150 °C and 300 °C, the surfactant decomposition generated a weight loss of 65%; and between 300 °C and 550 °C, the remaining surfactant was eliminated. So, the thermal treatment temperature selected was 600 °C to ensure the complete elimination of the surfactant.

The TGA was performed in the silica particles also after the thermal treatment; **Figures 3 and 4** presents the mass loss and its derivative versus temperature in nitrogen and air atmosphere respectively. In **Figure 3** it can be seen that the particles loss approximately 3 % of their mass until 100 ˚C which was associated with loss of moisture, and at higher temperatures there are no noticeable stages of mass loss. At 900 ˚C the residual mass was 95 %. In **Figure 4** it can be seen that the particles loss the 20% of their mass during the first 100 ˚C and the residual mass at the end of the test was 76%. Both tests denote the great thermal stability of the synthesized silica particles.

Unlike conventional crystalline structures, in the XRD pattern of a periodic mesoporous material, the diffraction peaks are related to a mesostructural order, which is observed at low angles (2θ) [22]. **Figure 5** shows the diffraction pattern of the mesoporous silica particles: a peak can be observed at 2θ=2.53. By applying Bragg´s law (λ=1.54 Å), a spacing d=3.49 nm was obtained. This value was associated with the distance between two empty pore channels, i.e. the mesopores spacing in the structure of the particles, and was coincident with values previously reported [17, 19, 23].

The FTIR test was done before and after the heat treatment to characterize the chemical structure of the surface of the particles (results are presented in **Figure 6)**. The peak

located between 2800 and 3000 cm^{-1} corresponds to the C-H bond, is associated with the micelles of the organic surfactant (CTAB) that were inside the mesopores and is expected to be eliminated. The absence of the peak in the treated samples confirmed that the thermal treatment was successful. Before and after the treatment, the peak situated at 1058 cm^{-1} corresponds to the Si-O-Si bond vibration.

The SEM images of the particles after heat treatment are presented in **Figure 7.** Some agglomeration can be observed, with particles in the order of microns and worm-like morphology.

The images obtained by TEM (**Figure 8**) confirmed the mesoporous structure and the coalescence of the particles**.** Measuring by software the dimensions of the spacing between channels the obtained values are in agreement with the XRD results, resulting in both techniques a spacing of about 3.4 nm.

3.2 Phenolic composites

The obtained composites are presented in **Figure 9**. The plates were analyzed by FTIR to compare the effect of the additives in the phenolic resin crosslinking. The methylene bridge bands placed at 1456 cm-^{1} (p-p') and 1473 cm^{-1} (o-p'), as well as the reference peak that was used for normalization (stretching of the ethylene bond C=C in the benzene ring at 1595 cm^{-1}) [20,21, 24, 25] are indicated in **Figure 10**. The relative heights of the mentioned peaks were taken as an indication of the degree of crosslinking of the materials and the results are presented in **Table 2**. The phenolic resin was taken as a reference and the increase or decrease in the peak height was considered as an increase or decrease of the crosslinking density. It was observed a reduction in the crosslinking density with the incorporation of both types of particles. This is because particles act as discontinuous points for the polymer network, decreasing the

crosslinking capacity. However, in the case of the silica particles, the reduction was slighter, which was attributed to the chemical interaction between the hydroxyl groups of the phenolic resin and the silanols of the silica particles [26]. This interaction can rigidize the network, mending some of the unbonded chains present in the polymer. The overall effect should be a decrease in the degradation temperature (the interaction is not as strong as a covalent bond) but with a decrease of the mobility of the polymer chains, which in turn produces an increase in the T_g. As seen later, TGA and DMA results confirmed that hypothesis.

The thermal behavior of the materials was studied by thermogravimetry under a nitrogen atmosphere. The curves of weight loss and its derivative versus temperature are presented in **Figure 11 a and b**. It can be observed that the weight loss stages are either similar or slightly shifted to lower temperatures when compared to the neat phenolic resin with the modified ones, that is, neither of the added reinforcements in 5 or 20 wt. % improved the resin thermal stability. A similar behavior was observed by Ding *et al.* for phenolic modified with zirconium silicide particles [27]. Regarding the residual mass, a different behavior was observed for the different systems studied: carbon black composites showed the highest residual mass, which indicates that carbon black favored the formation of the carbonaceous residue. This is desirable because char formation is one of the main mechanisms for thermal resistance in high temperature application. It is worth mentioning that TGA is a small-scale test with controlled parameters such as heating rate and atmosphere, and that the results cannot fully characterize composite behavior with respect to ablation. The ablative properties should be evaluated by the torch test.

The microstructure of the composites and the dispersion of the reinforcements in the phenolic matrix were studied by TEM. Only the images of the composites with the

highest filler content (20 wt. %) were analyzed for both type of nanoparticles. The photographs are showed in **Figure 12 a and b**. Carbon black particles are spherical aggregates of about 300 nm in size and each aggregate is made up of elementary particles of about 50 nm. A good dispersion and the mentioned structure can be seen in the TEM images. In the materials with silica particles, mesoporosity is clearly seen, and darker areas correspond to overlapping of two or more particles. A good dispersion in the phenolic resin was confirmed.

DMA was conducted to analyze the network structure and the compatibility between the matrix and the reinforcement, based on the evolution of storage and loss moduli rate (tanδ) as temperature is increase (**Figure 13**). The temperature at tanδ peak is the T_g of the material, while its height (damping) is related to the crosslinking degree (the higher the peak, the lower the crosslinking degree). The obtained values of damping are in agreement with the tendency observed in FTIR studies (**Table 3**). Both carbon black and silica particles reduce crosslinking density, being the reduction stronger in the first case. The glass transition temperature was higher for the system with mesoporous silica particles and lower for the carbon black system. The better compatibility with a rigid reinforcement reduced the mobility of the non-crosslinked chains in the interphase, increasing T_g.

To evaluate the ablation resistance of the materials, it is necessary to simulate the aggressive conditions of the hyper-thermal environment to which thermal protection systems are subjected (high heat fluxes and very high temperatures). The oxyacetylene torch test (ASTM E285) is commonly used to measure the ablative resistance of materials at a laboratory scale. The experimental set-up is presented in **Figure 14**. Plates were situated at 1.9 cm of the torch and the flame was controlled by changing the oxygen and acetylene proportion. The information of the temperature rise versus time

was acquired with a thermocouple located in the back side of the samples. The test consists in exposing the sample to the flame and recording the time that it takes to be passed through. From that time, the erosion rate was calculated with **Eq. 1 and 2** and results are presented in **Figure 15.** The global effect of particle incorporation is the result of two opposite contributions: the observed reduction in the crosslinking density for both types of particles should decrease the ablation resistance of the composites (the pyrolysis is facilitated), while the increase in particle amount should increase the ablation resistance due to its better thermal properties. In consequence, there is an initial increase in the erosion rate at low particle concentrations, but at high load levels the better thermal resistance and low thermal conductivity of the particles produce the decrease of the erosion rate of the composites. The material with 20 wt. % of mesoporous silica particles showed the lowest erosion rates, and the reduction was higher when comparing the erosion rate in terms of mass loss. This indicates that the particles act reducing the affected area by the flame, which in a real application (protection of a nozzle of rocket engines) leads to higher protection times. The degree of degradation in zones far from the flame depends not only on the degradation resistance itself but also on the thermal conductivity and the thermal diffusivity of the composite. Insulation indexes are used to compare the capacity of insulation between different materials. Basically compare the time that the material takes to reach fixed temperatures. Are suggested to be calculated in the ASTM 285 standard with **Eq. 3**.

$$Linear\ erosion\ rate = \frac{d}{t} \qquad \textbf{(Eq. 1)}$$

where:

d = thickness of the specimen [m]

t = burn-through time [s]

$$Mass\ erosion\ rate = \frac{(m_i - m_f)}{t} \qquad \textbf{(Eq. 2)}$$

where:

m_i = initial mass of the specimen [g]

m_f = final mass of the specimen [g]

t = burn-through time [s]

$$I_T = \frac{t_T}{d} \qquad \textbf{(Eq. 3)}$$

where:

I_T = insulation index at temperature T [s/m]

t_T = time for back-face temperature changes of 80, 180, and 380 °C [s]

d = thickness of specimen [m]

Table 4 summarizes the results of insulation indices**,** while **Figure 16** compares representative temperature vs time (normalized by thickness) curves. The silica nanocomposites showed the best performance since the temperature rise was delayed to longer times. In contrast to what happened with the erosion rates, the effect of increasing insulation indices was marked even at low filler loads. Therefore, high particle loads are needed to reduce the erosion and degradation rate, but low particle concentrations are enough to enhance the insulation capability. The better insulation of the silica nanocomposites is a consequence of the low conductivity of the mesoporous structure of the particles.

The carbonaceous residue formed during the torch test for the materials with 20 wt. % of reinforcements was studied by SEM. **Figure 17** shows four images of each material, each with higher magnification. In the case of the neat phenolic resin, the plates had almost no integrity, and a morphology of grains that become smaller when they are closer to the flame can be observed. Micro- and macro-cracks were formed, and the materials failed because of its coalescence. The image with higher magnification looks like a texture of 'orange peel' [28] formed by the vaporization of water and the generation of volatiles. The material with carbon black **(b)** had macro-cracks that were generated by the contraction during the processing and after the fire generated a grain morphology. The figure with the highest magnification shows some carbon black particles within the degraded matrix.

Unlike the other materials, the plates with mesoporous silica particles **(c)** presented a white color after the exposure to the flame. The images show the presence of cracks and their intersections, as well as some bright points placed on the surface, which were attributed to amorphous silica spheres generated during the torch test [19]. With higher magnification, some silica particles that remained after the fire can be seen without traces of resin. A very important aspect to consider is that the zones generated from the mesoporous silica particles remain on the surface despite the erosion generated during the test flame. This would explain why the resistance to ablation of this material is increased.

4. CONCLUSIONS

In this work, a new strategy to increase the ablation resistance of phenolic resin by means of incorporation of mesoporous silica particles was studied. The particles were synthesized by sol-gel and characterized in terms of chemical structure (FTIR, TGA) and morphology (SEM, TEM, XRD). Once the synthesis was optimized, particles were

incorporated to the resin at two concentrations (5 and 20%). Also, carbon black-modified resins were prepared to compare the performance with that obtained with the filler commonly used in ablative resistance composites. Composites were characterized by TGA, DMA, FTIR and TEM and the burned ones with an oxyacetylene torch test. The burned plates were studied by SEM. Infrared spectra and DMA results showed that carbon black has low compatibility with the phenolic resin (crosslinking degree and T_g are reduced) but favors the formation of the carbonaceous residue, increasing the residual mass in the TGA tests. On the other hand, the silica particles increased the T_g and crosslinking density, which is an indication of the good particle/matrix compatibility. Both kinds of particles reduced the erosion rate during the ablation tests. High loadings were necessary to obtain a significant increase in the ablation resistance of the composites. In addition, the degree of insulation increased with the addition of both carbon black and silica particles. The best performance was obtained for composites with 20% of silica particles, being the mesoporous structure and the thermal resistance (attributed to the high silica obtained in the sol-gel process) the ones responsible for the enhanced ablation performance.

The excellent results discovered encouraged the development of carbon fiber reinforced composites employing these improved matrices, as a continuation of the research in which the author´s are working.

Acknowledgements

The authors would like to thank to the National Council of Scientific and Technical Research (CONICET), The National University of Mar del Plata and National Agency of Scientific and Technological Promotion, ANPCyT (grant code PICT 2013 2455).

References

[1] Natali M, Puri I, Kenny JM, Torre L, Rallini M. Microstructure and ablation behavior of an affordable and reliable nanostructured Phenolic Impregnated Carbon Ablator (PICA). Polymer Degradation and Stability 141, 84-96 (2017).

[2] Natali M, Monti M, Puglia D, Kenny JM, Torre L. Ablative properties of carbon black and MWNT/phenolic composites: A comparative study. Composites: Part A 43, 174–182 (2012).

[3] Koo JH, Pilato LA, Wissler GE. Polymer Nanostructured Materials for Propulsion Systems. Journal of spacecraft and rockets, Vol. 44, No. 6, (2007). DOI: 10.2514/1.26295.

[4] Cheng H, Xue H, Hong C, Zhang X. Preparation, mechanical, thermal and ablative properties of lightweight needled carbon fibre felt/phenolic resin aerogel composite with a bird's nest structure. Composites Science and Technology 140, 63-72 (2017).

[5] Natali M, Kenny JM, Torre L. Science and technology of polymeric ablative materials for thermal protection systems and propulsion devices: A review. Progress in Material Science 84, 192-275 (2016).

[6] Natali M, Rallini M, Kenny JM, Torre L. Effect of Wollastonite on the ablation resistance of EPDM based elastomeric heat shielding materials for solid rocket motors. Polymer Degradation and Stability 130, 47-57 (2016).

[7] Chena S, Lib G, Hua H, Lia Y, Meic M. Microstructure and properties of ablative C/ZrC–SiC composites prepared by reactive melt infiltration of zirconium and vapour silicon infiltration. Ceramics International 43, 3439–3442 (2017).

[8] Triantou K, Mergia K, Florez S, Perez B, Barcena J, Rot€armel W, Pinaud G. Thermo-mechanical performance of an ablative/ceramic composite hybrid thermal protection structure for re-entry applications. Composites Part B 82, 159-165 (2015).

[9] Jayaseelan DD, Xin Y, Vandeperre L, Brown P, Lee WE. Development of multi-layered thermal protection system (TPS) for aerospace applications. Composites Part B 79, 392-405 (2015).

[10] Bassyouni M, Iqbal N, Iqbal SS, Abdel-hamid SM-S., Abdel-Aziz MH, Javaid U, Bilal Khan M. Ablation and thermo-mechanical investigation of short carbon fiber impregnated elastomeric ablatives for ultrahigh temperature applications. Polymer Degradation and Stability 110, 195-202 (2014).

[11] Wang ZJ, Kwon DJ, Gu GY, Lee WI, Park JK, DeVries JK, Park JM. Ablative and mechanical evaluation of CNT/phenolic composites by thermal and microstructural analyses. Composites: Part B 60, 597–602, (2014).

http://dx.doi.org/10.1016/j.compositesb.2013.12.042.]

[12] Pulci G, Tirillò J, Marra F, Fossati F, Bartuli C, Valente T. Carbon–phenolic ablative materials for re-entry space vehicles: Manufacturing and properties. Composites: Part A 4, 1483–1490 (2010). doi:10.1016/j.compositesa.2010.06.010.

[13] Koo JH, Stretz J, Weispfenning JT, Luo Z, Wootan W. Nanocomposite Rocket Ablative Materials: Processing, Microstructure, and Performance. 45th AIAA/ASME/ASCE/AHS/ASC Structures, Structural Dynamics & Materials Conference April 2004, Palm Springs, California.

[14] Mirzapour A, Asadollahi MH, Baghshaei S, Akbari M. Effect of nanosilica on the microstructure, thermal properties and bending strength of nanosilica modified carbon fiber/phenolic nanocomposite. Composites: Part A 63, 159–167 (2014).

[15] Balaji R, Sasikumar M, Elayaperumal A. Thermal, thermo oxidative and ablative behavior of cenosphere filled ceramic/phenolic composites. Polymer Degradation and Stability 114, 125-132 (2015).

[16] Natali M, Monti M, Kenny JM, Torre L. A nanostructured ablative bulk molding compound: Development and characterization. Composites: Part A 42, 1197–1204 (2011).

[17] Bippus L, Jaber M, Lebeau B, Schleich D, Scudeller Y. Thermal conductivity of heat treated mesoporous silica particles. Microporous and Mesoporous Materials, 190, 109–11 (2014). http://dx.doi.org/10.1016/j.micromeso.2014.02.006.

[18] Cooper C, Burch R. Mesoporous materials for water treatment process. Water Research, Vol. 33, No. 18, pp. 3689±3694 (1999).

[19] Xie M, Shi H, Ma K, Shen H, Li B, Shen S, Wang X, Jin Y. Hybrid nanoparticles for drug delivery and bioimaging: Mesoporous silica nanoparticles functionalized with carboxyl groups and a near-infrared fluorescent dye. Journal of Colloid and Interface Science 395 306–314, (2013).

[20] Asaro L, Rivero G, Manfredi LB, Álvarez VA, Rodríguez ES. Development of carbon fiber/phenolic resin prepregs modified with nanoclays. Journal of Composite Materials, 50 (10) pp. 1287 – 1300 (2016). DOI: 10.1177/0021998315590866.

[21] Manfredi LB, de la Osa O, Galego Fernández N, Vázquez A. Structure-properties relationship for resols with different formaldehyde/phenol molar ratio. Polymer 40, 3867–3875 (1999).

[22] Qian Y, Wei P, Jiang P, Li Z, Yan Y, Ji K. Aluminated mesoporous silica as novel high-effective flame retardant in polylactide. Composites Science and Technology 82, 1–7 (2013). http://dx.doi.org/10.1016/j.compscitech.2013.03.019.

[23] Trewyn BG, Slowing II, Giri S, Chen HT, Lin VSY. Synthesis and Functionalization of a Mesoporous Silica Nanoparticle Based on the Sol–Gel Process and Applications in Controlled Release. Accounts of Chemical Research 40, 846–853 (2007). DOI: 10.1021/ar600032u.

[24] Rocniak C, Biernacka T, Skarzynski M. Some properties and chemical structure of phenolic resins and their derivatives. Journal of Applied Polymer Science, 28, 531 (1983).

[25] Lum R, Wilkins CW, Robbins M, Lyons AM, Jobes RP. Thermal analysis of graphite and carbon-phenolic composites by pyrolysis-mass spectrometry. Carbon, 21(2):111–6 (1983).

[26] Lin JM, Ma CCM. Thermal degradation of phenolic resin/silica hybrid ceramers. Polymer Degradation and Stability 69, 229-235 (2000).

[27] Ding J, Huang Z, Qin Y, Shi M, Huang C, Mao J. Improved ablation resistance of carbon phenolic composites by introducing zirconium silicide particles. Composites Part B 82, 100-107 (2015). http://dx.doi.org/10.1016/j.compositesb.2012.11.007.

[28] Bouslah M, Salvia M, Deschères I, Berthel B, Benayoun S. Effect of microsphere content on fire performance and termomechanical properties of phenolic resole syntactic

foam composites. The 19Th International Conference on Composite Materials, pp 4531-4542 (2013).

Figures

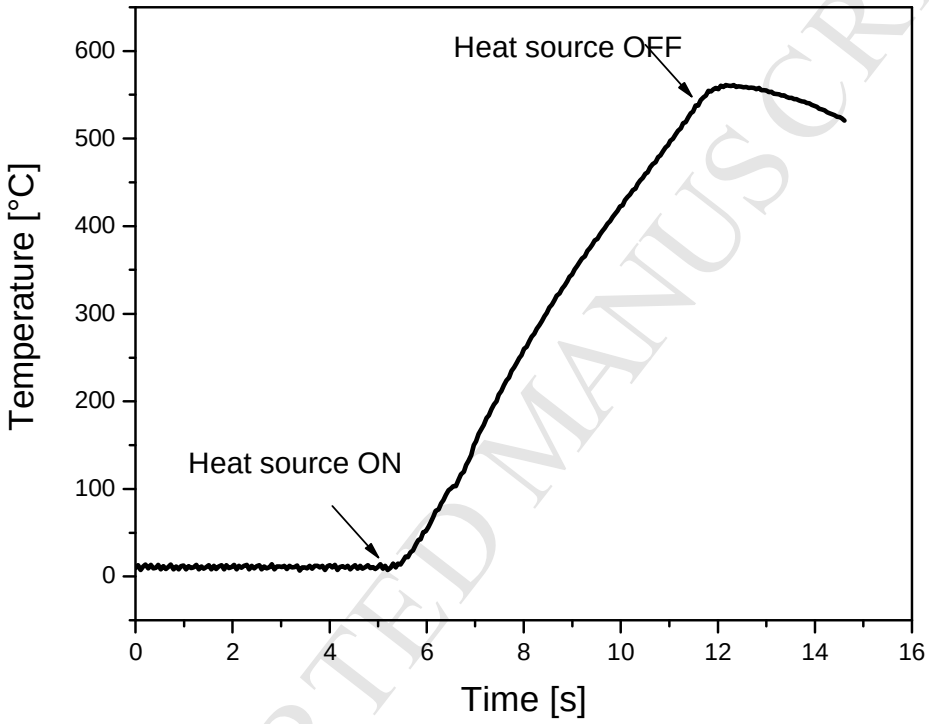

Figure 1. Temperature as a function of time obtained during the measurement of heat-transfer rate in the oxyacetylene torch equipment.

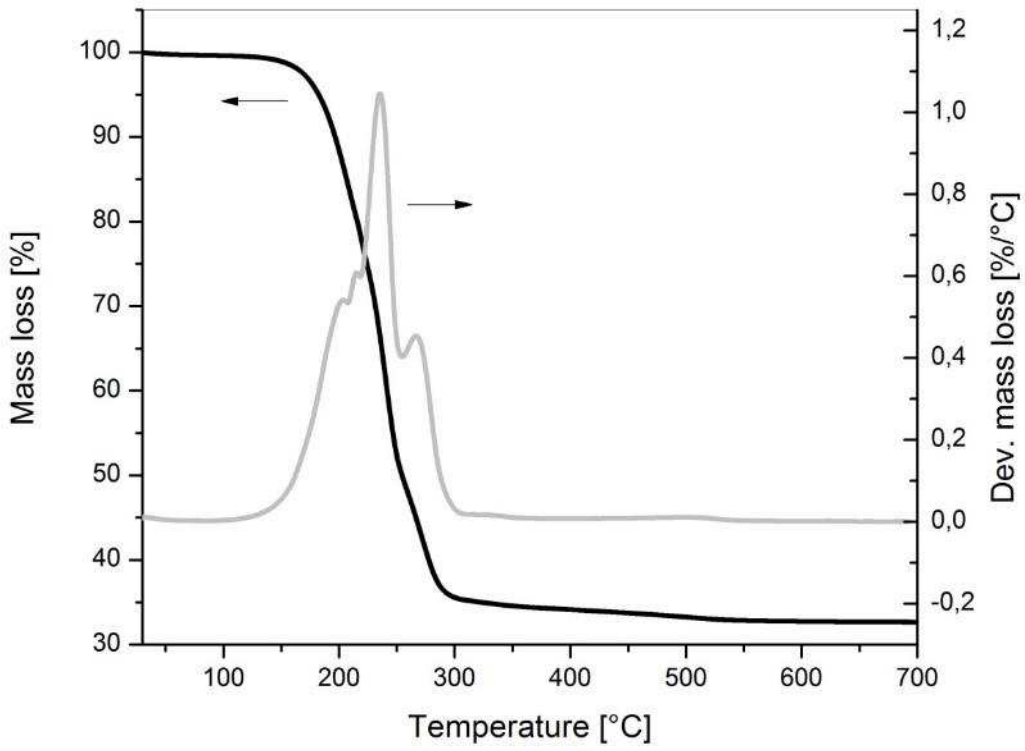

Figure 2. Mass loss and its derivative as a function of temperature, obtained at 10 ˚C/min in nitrogen atmosphere for mesoporous silica particles before heat treatment.

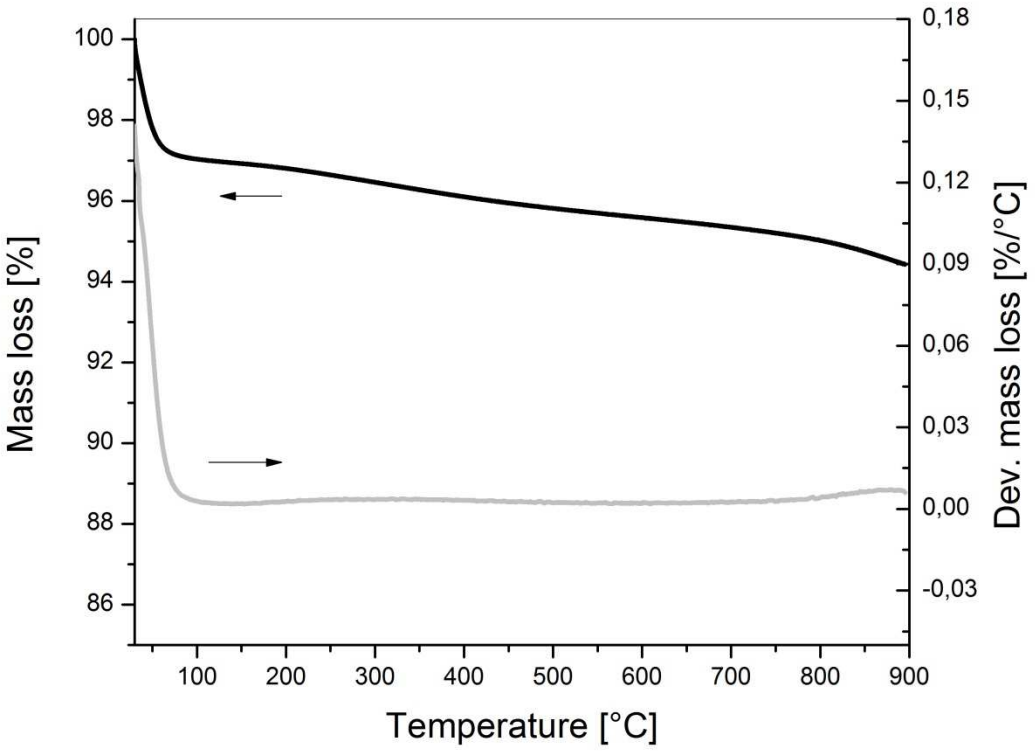

Figure 3. Mass loss and its derivative as a function of temperature, obtained at 10 ˚C/min in nitrogen atmosphere for mesoporous silica particles after heat treatment.

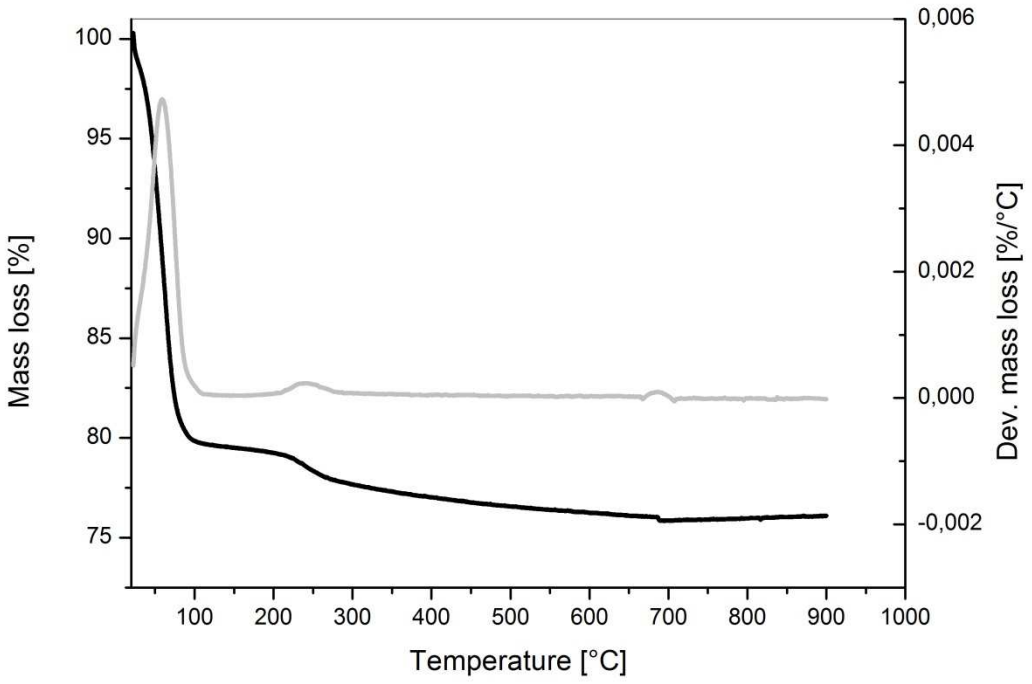

Figure 4. Mass loss and its derivative as a function of temperature, obtained at 10 ˚C/min in air atmosphere for mesoporous silica particles after heat treatment.

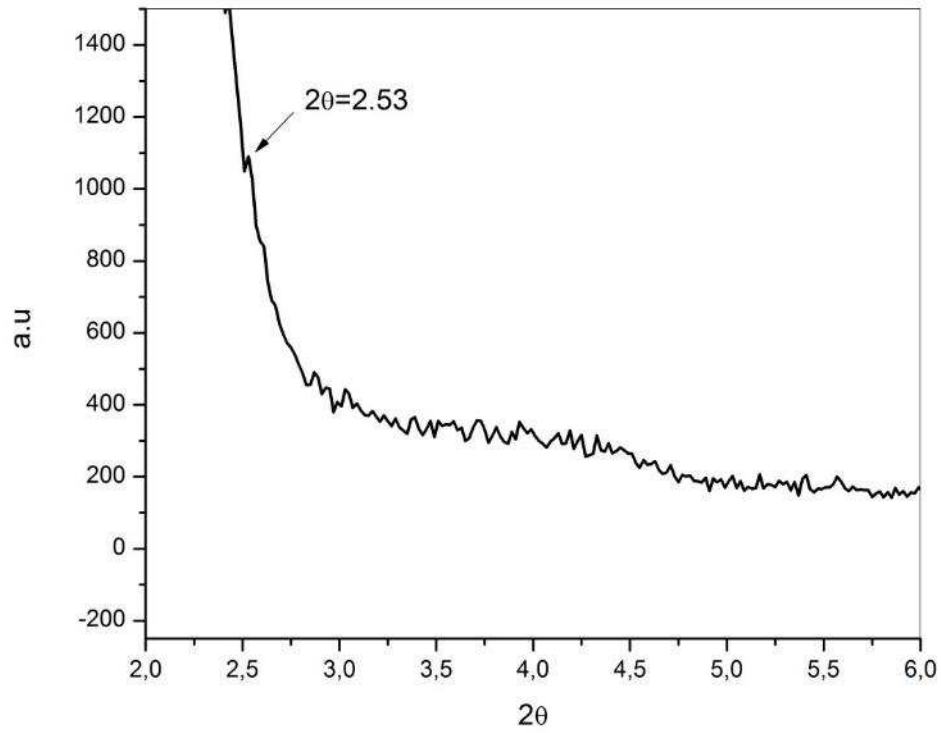

Figure 5. XRD Pattern of mesoporous silica particles after heat treatment at 600 ˚C.

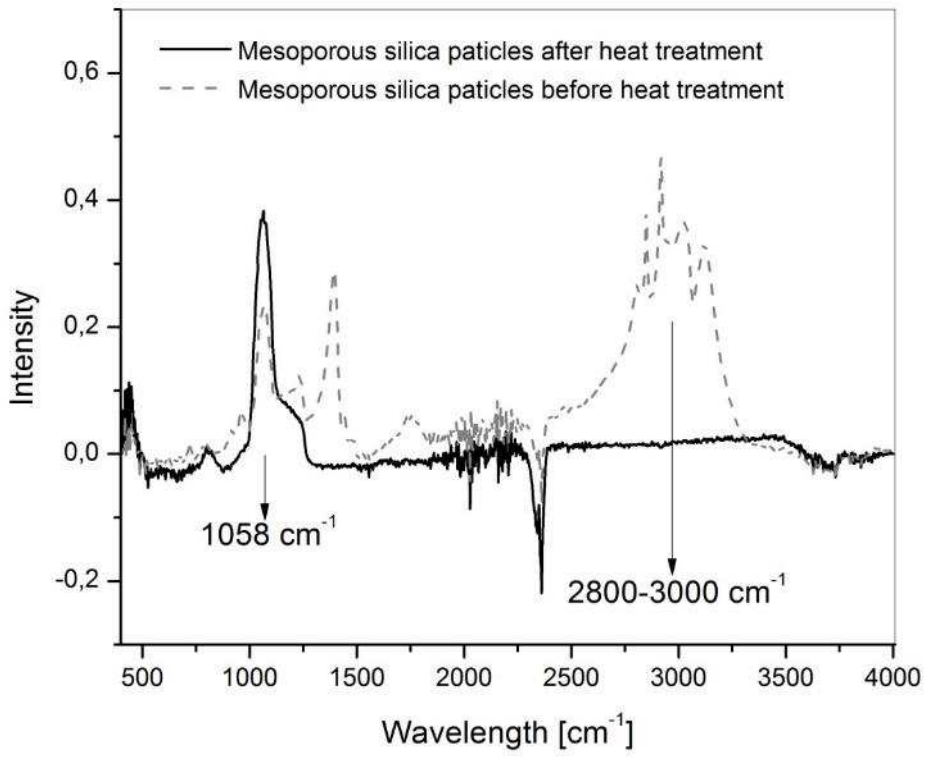

Figure 6. FTIR spectra of the mesoporous silica particles before and after heat treatment.

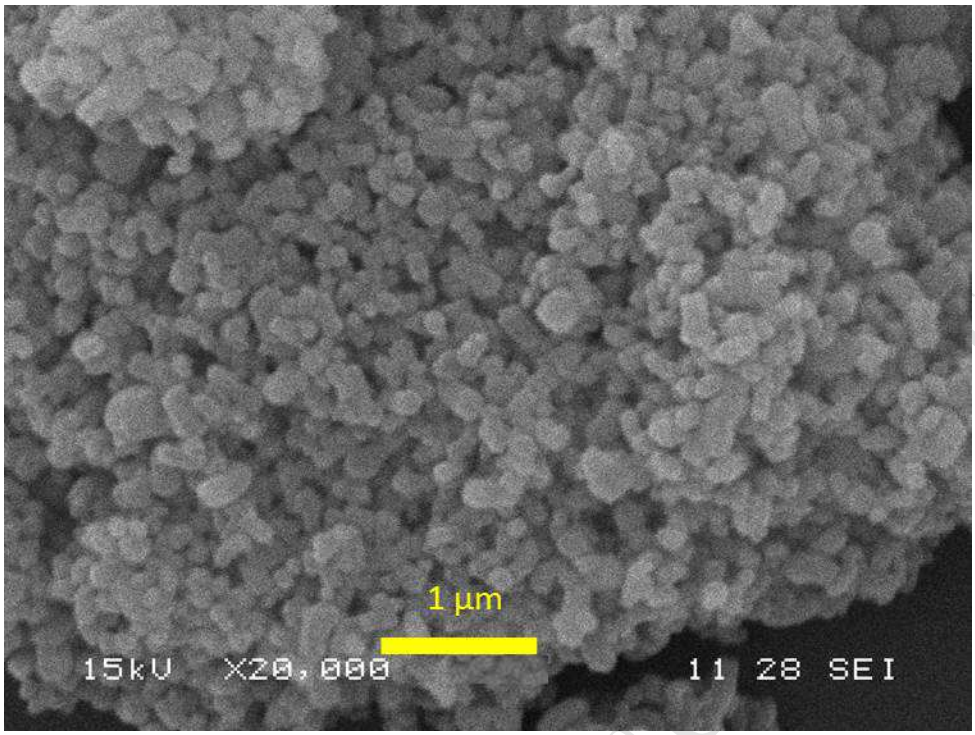

Figure 7. SEM images of the mesoporous silica particles after heat treatment at 600 ˚C.

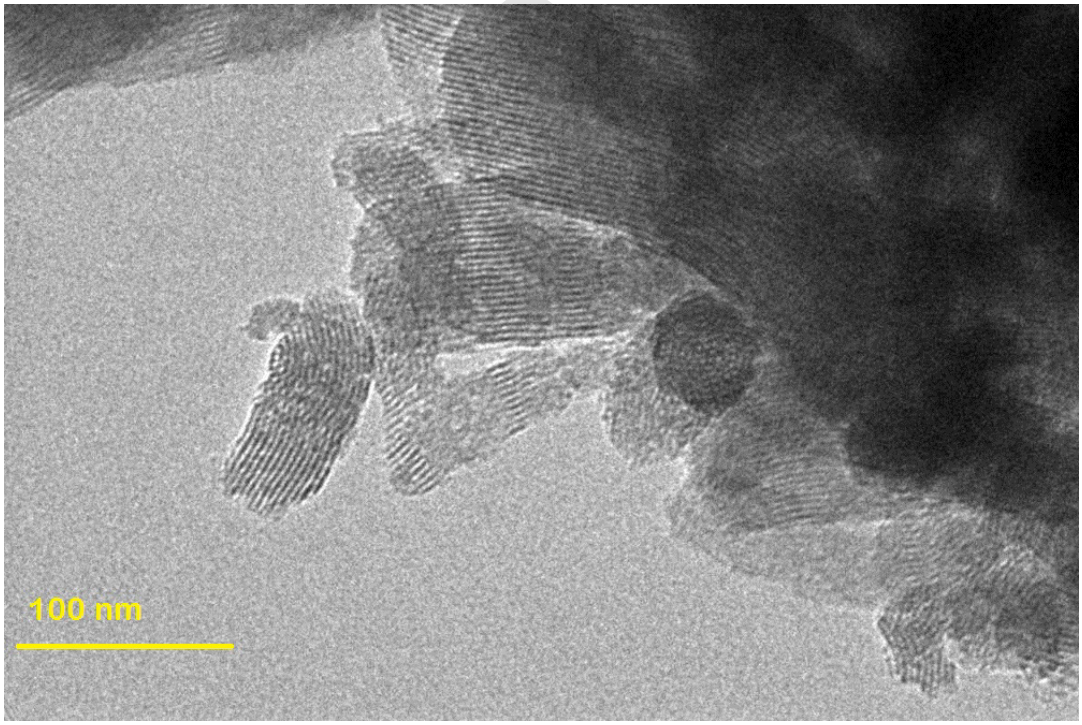

Figure 8. TEM image of the mesoporous silica particles after heat treatment at 600 ˚C.

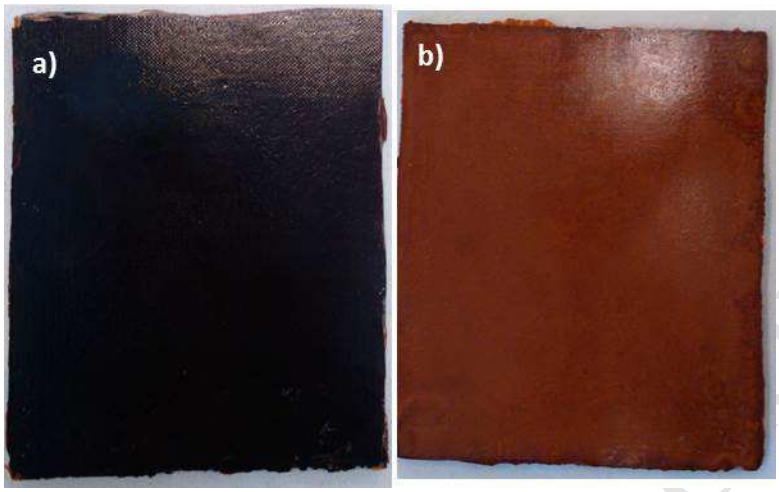

Figure 9. Plates of the obtained nanocomposites **a)** Phenolic resin with wt. % of carbon black, **b)** Phenolic resin with 20 wt. % of mesoporous silica particles.

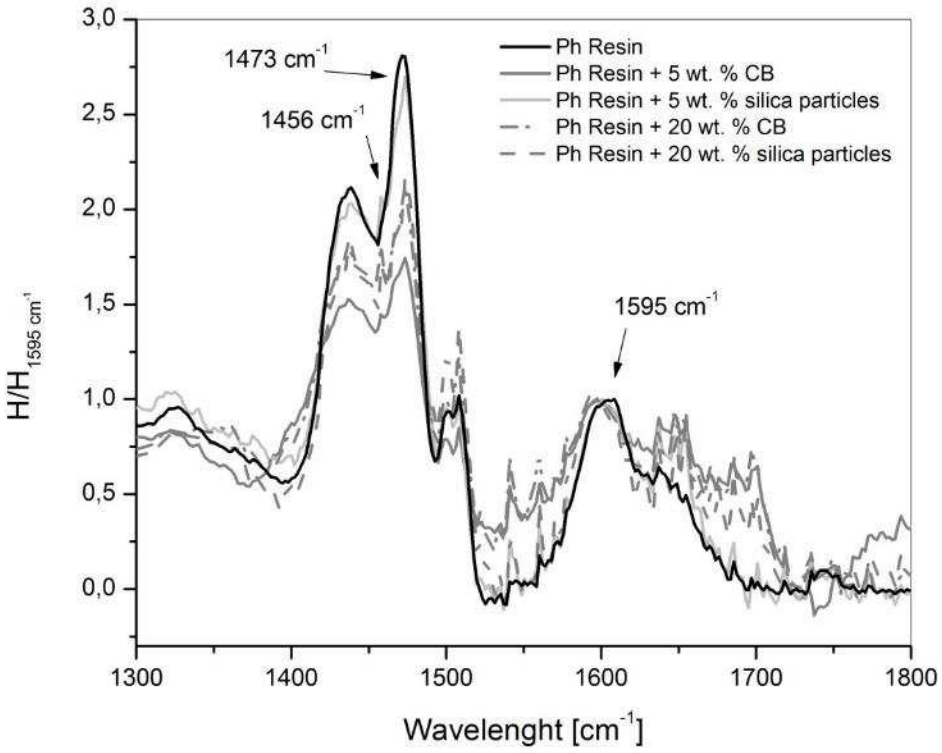

Figure 10. Nanocomposites normalized FTIR spectra in the 1300-1800 cm^{-1} range, methylene bridges bands are placed at 1456 cm^{-1} (p-p') and 1473 cm^{-1} (o-p').

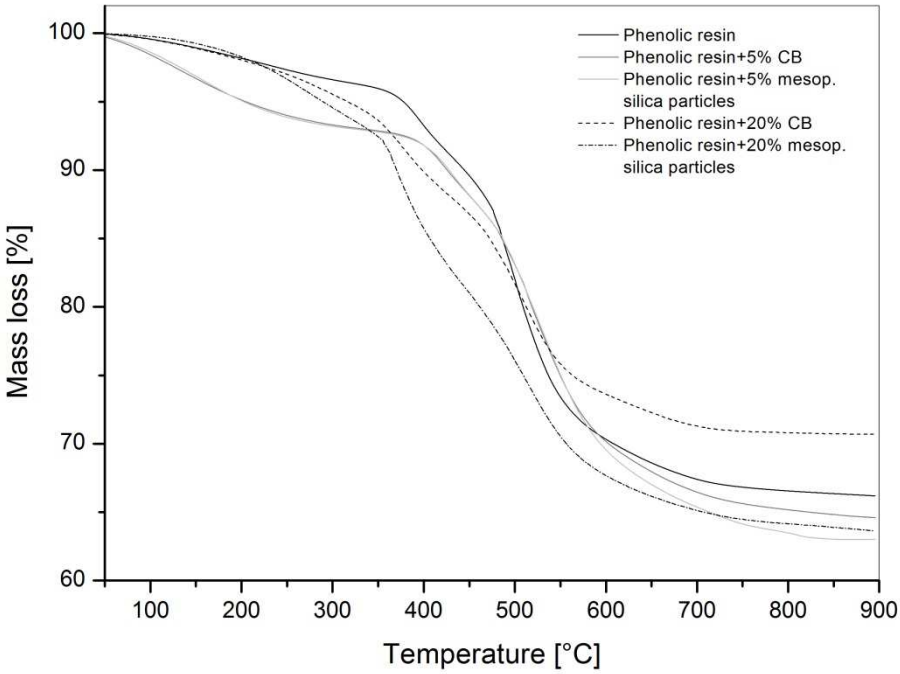

Figure 11. a) Mass loss as a function of temperature, obtained at 10 ˚C/min in nitrogen atmosphere for the obtained nanocomposites based on phenolic resin with carbon black and mesoporous silica particles.

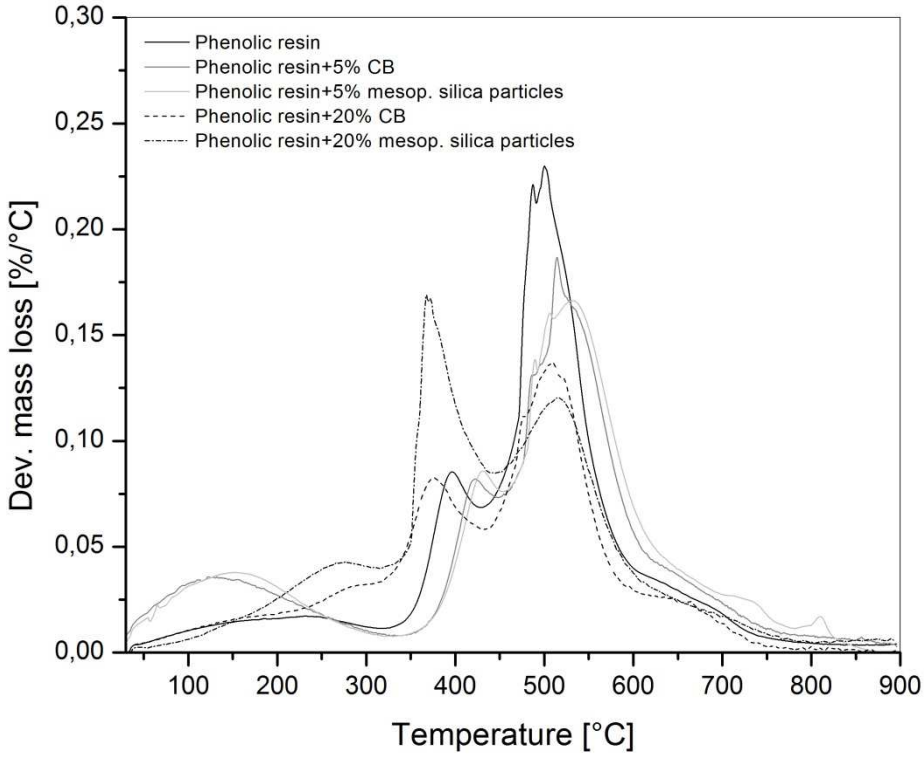

Figure 11. b) Mass loss derivative as a function of temperature, obtained at 10 ˚C/min in nitrogen atmosphere for the obtained nanocomposites based on phenolic resin with carbon black and mesoporous silica particles.

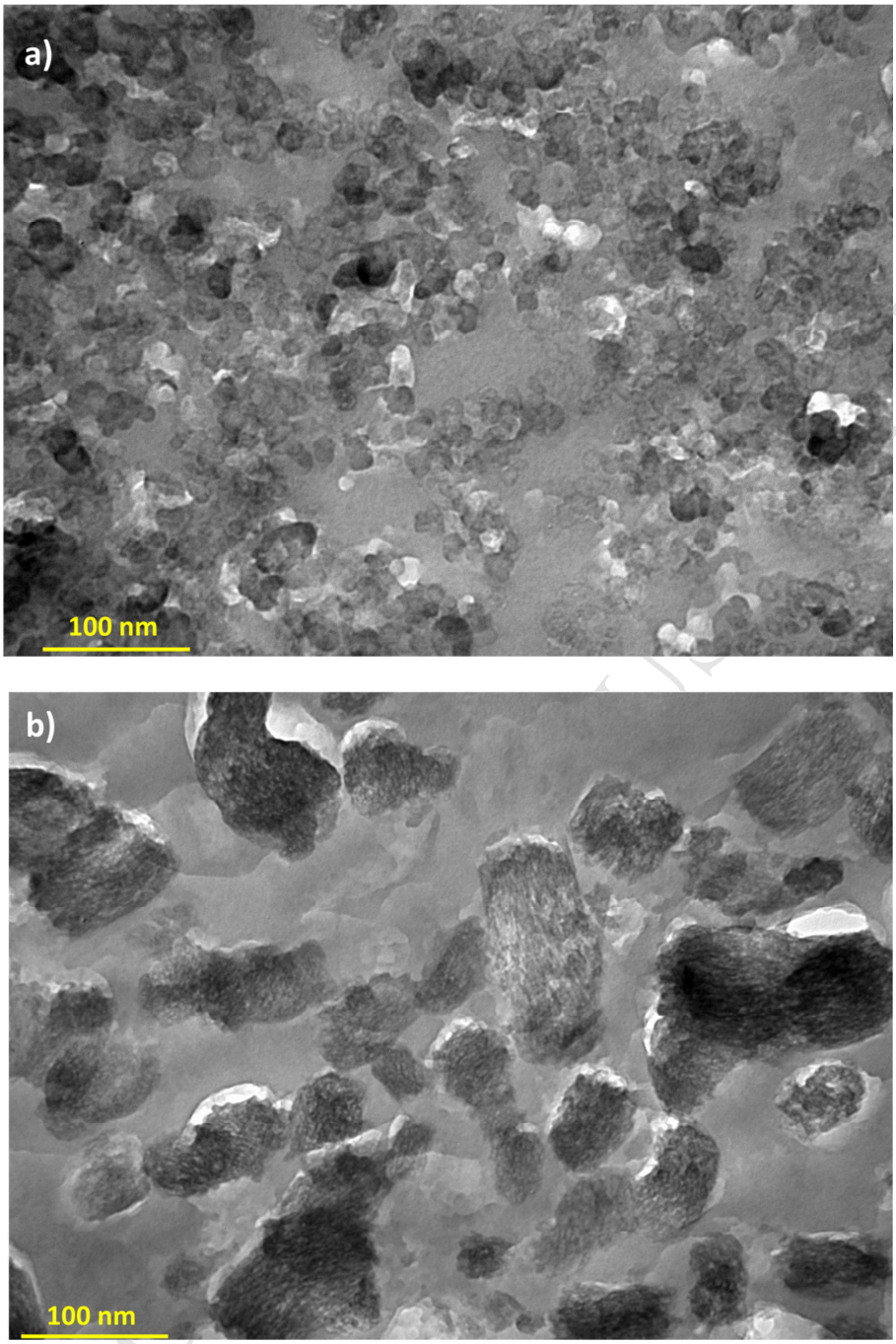

Figure 12. TEM images of the nanocomposites with a) 20 wt. % of carbon black, b) 20 wt. % of mesoporous silica particles.

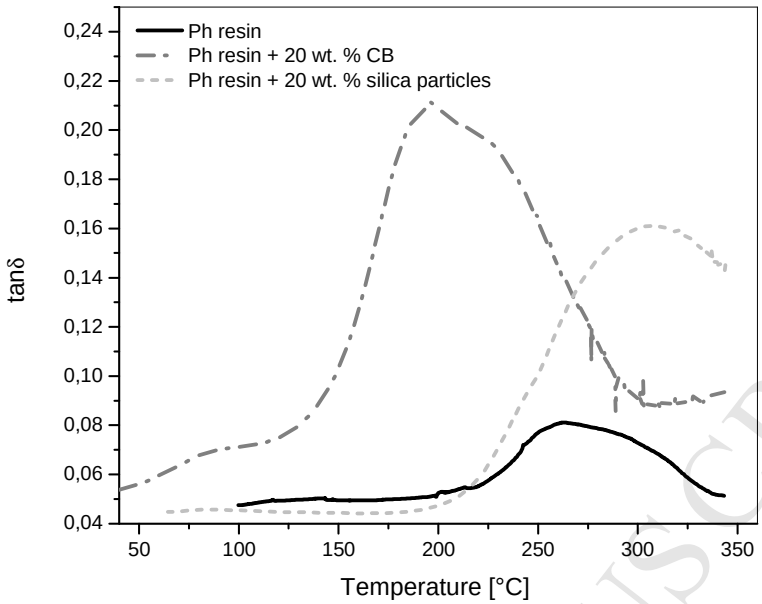

Figure 13. tanδ versus temperature curves obtained by DMA, from 30 to 350 °C at a heating rate of 5 °C/min.

Figure 14. Oxyacetylene torch test equipment scheme.

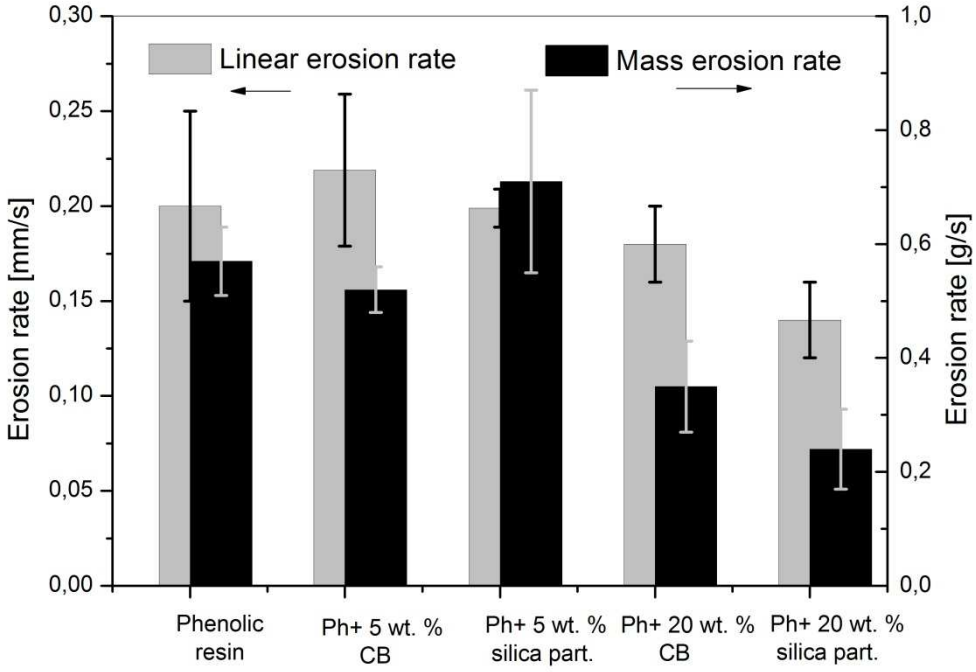

Figure 15. Erosion rate for each nanocomposite obtained in the oxyacetylene torch test.

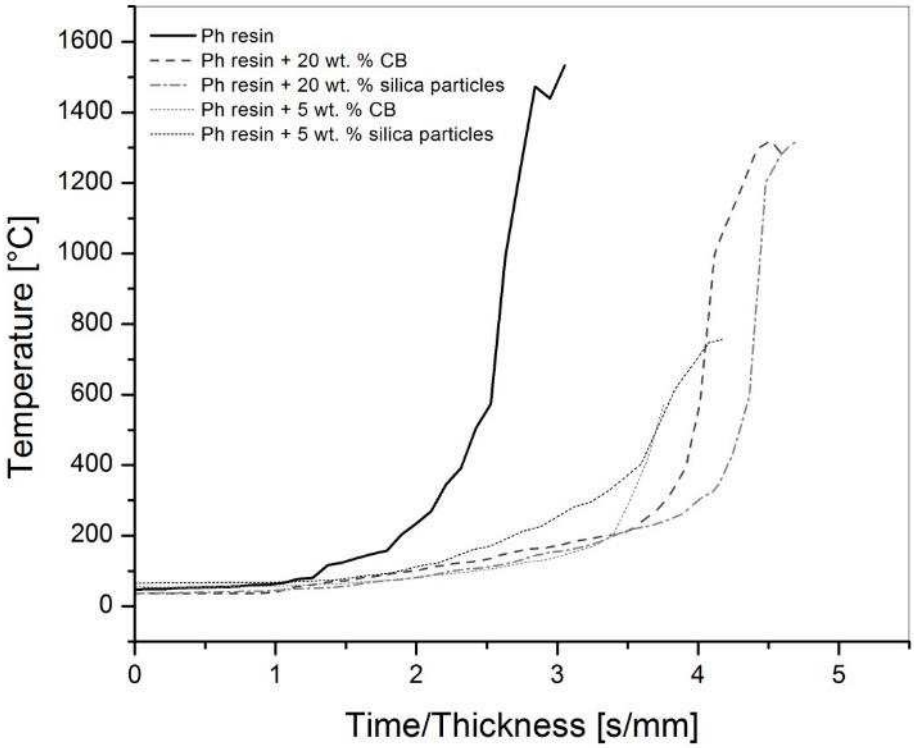

Figure 16. Temperature rise on the back face of the materials during the torch test.

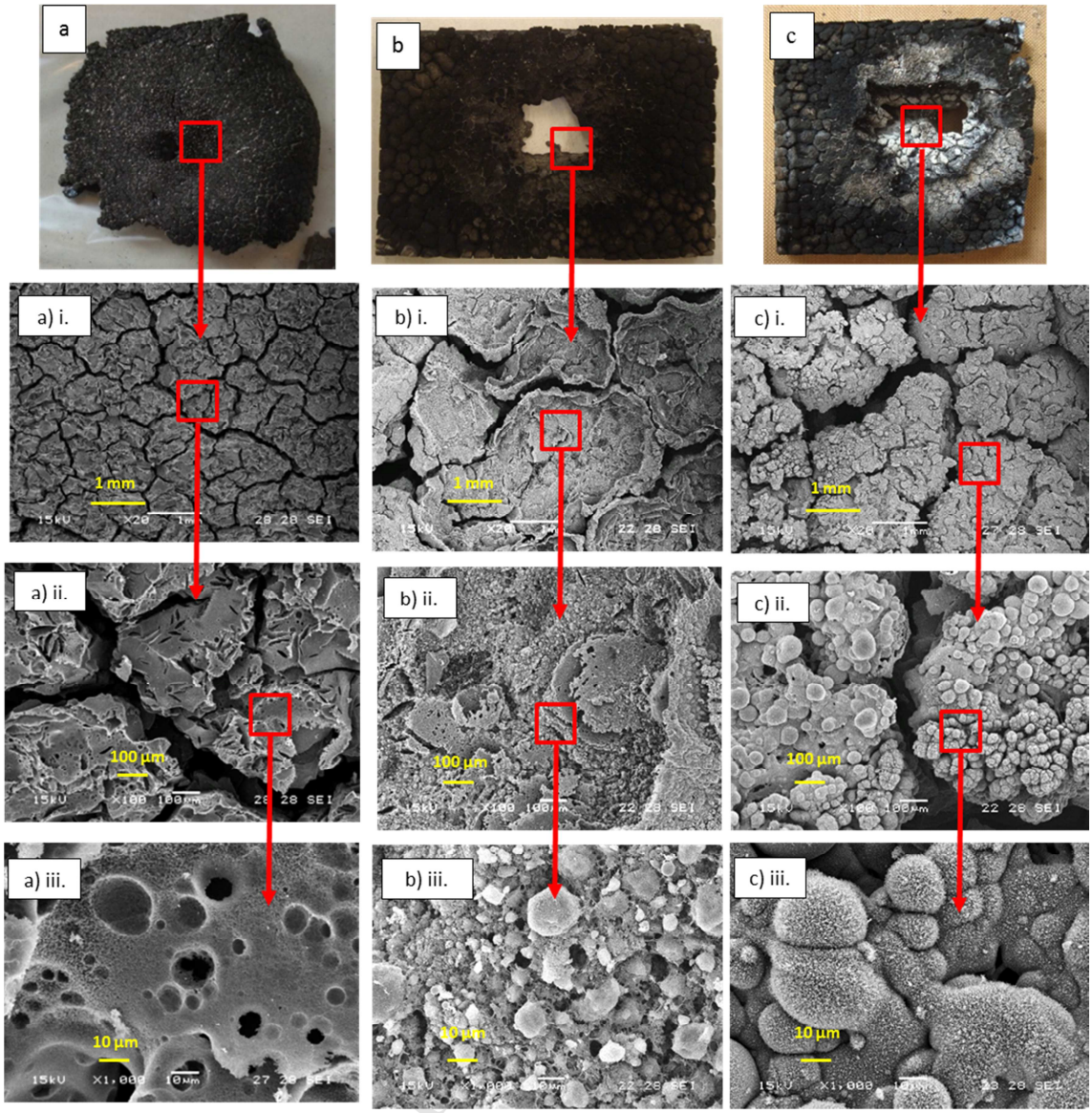

Figure 17. SEM images of the burned samples a) Phenolic resin, b) Phenolic resin with 20 wt. % of carbon black, c) Phenolic resin with 20 wt. % of mesoporous silica particles. i) 20 x, ii) 100 x iii) 1000 x.

Tables

Property	Value
Viscosity at ambient temperature	1200 cp
Solid content	78 %
Gel time at 80 ˚C	More than 4 h
Gel time at 100 ˚C	2 h 57 min
Gel time at 120 ˚C	41 min
Gel time at 140 ˚C	18 min

Table 1. Used phenolic resin characteristics.

Material / $-CH_2-$ bridge	p-p'	o-p'
Phenolic resin	1.81	2.8
Phenolic resin with 5 wt. % of carbon black	1.44	1.64
Phenolic resin with 5 wt. % of silica particles	2.00	2.69
Phenolic resin with 20 wt. % of carbon black	1.36	1.39
Phenolic resin with 20 wt. % of silica particles	1.70	2.16

Table 2. Relative magnitude of the methylene bridges peaks.

Material	T peak of tanδ (T_g) [°C]	Height of tanδ peak
Phenolic resin	269	0.08
Phenolic resin with 5 wt. % of carbon black	286	0.15
Phenolic resin with 5 wt. % of silica particles	287	0.12
Phenolic resin with 20 wt. % of carbon black	200	0.2
Phenolic resin with 20 wt. % of silica particles	316	0.16

Table 3. Glass transition temperature and height of tanδ peak obtained by DMA.

Material	I_{80}* [s/mm]	I_{180}* [s/mm]	I_{380}* [s/mm]
Phenolic resin	1.36 ± 0.53	1.86 ± 0.55	2.16 ± 0.45
Phenolic resin with 5 wt. % of carbon black	1.14 ± 0.84	2.44 ± 0.78	3.76 ± 0.92
Phenolic resin with 5 wt. % of silica particles	1.69 ± 0.13	2.63 ± 0.07	3.38 ± 0.19
Phenolic resin with 20 wt. % of carbon black	1.40 ± 0.29	2.91 ± 0.26	3.83 ± 0.04
Phenolic resin with 20 wt. % of silica particles	1.92 ± 0.09	3.43 ± 0.18	4.14 ± 0.07

* Insulation index at 80, 180 and 380 °C

Table 4. Insulation index calculated from the oxyacetylene torch test.